International Journal of Pharmaceutics 393 (2010) 219–229

Contents lists available at ScienceDirect

International Journal of Pharmaceutics

journal homepage: www.elsevier.com/locate/ijpharm

Pharmaceutical Nanotechnology

Chitosan–magnesium aluminum silicate nanocomposite films: Physicochemical characterization and drug permeability

Wanwisa Khunawattanakul[a], Satit Puttipipatkhachorn[b], Thomas Rades[c], Thaned Pongjanyakul[a,*]

[a] Faculty of Pharmaceutical Sciences, Khon Kaen University, 123 Mittraphap Road, Khon Kaen 40002, Thailand
[b] Department of Manufacturing Pharmacy, Faculty of Pharmacy, Mahidol University, Bangkok 10400, Thailand
[c] School of Pharmacy, University of Otago, PO Box 913, Dunedin, New Zealand

ARTICLE INFO

Article history:
Received 11 January 2010
Received in revised form 16 March 2010
Accepted 8 April 2010
Available online 14 April 2010

Keywords:
Chitosan
Magnesium aluminum silicate
Nanocomposite film
Heat treatment
Drug permeability

ABSTRACT

Chitosan–magnesium aluminum silicate (CS–MAS) films were prepared and the effects of MAS content and heat treatment of the CS–MAS dispersion before film casting on the physicochemical and drug permeability properties of the films were investigated. CS could interact with MAS via electrostatic interaction and intermolecular hydrogen bonding mechanisms, resulting in nanocomposite formation, for which it was not necessary to apply the heat treatment on the composite dispersions. The nature of the exfoliated and intercalated nanocomposite films formed was depended on the MAS content added. The heat treatment on the composite dispersions caused an increase in tensile strength, but reduced %elongation of the CS–MAS nanocomposite films. The exfoliated nanocomposite films showed higher flexibility, water uptake, and drug permeability compared to the CS and intercalated CS–MAS nanocomposite films. At higher MAS content, the CS–MAS films prepared using heat treatment had a lower water uptake, resulting in lower drug permeability when compared with those prepared using non-heated dispersions. The permeation mechanism of non-electrolyte and negatively charged drugs across the CS–MAS nanocomposite films was predominantly controlled by diffusion in water-filled microchannels, whereas both adsorption onto MAS and diffusion processes occurred concurrently for the film permeation of positively charged drugs. The findings of this study suggest that CS–MAS nanocomposite films can be formed without heating of the composite dispersion before casting. CS–MAS nanocomposites showed strong potential to be used as a film former for coated tablets intended for modulating drug release.

1. Introduction

Chitosan (CS) is a polysaccharide that consists of N-acetyl-D-glucosamine and D-glucosamine. CS is insoluble at neutral and alkaline pH since its pK_a is in the range of 6.2–7.0 (Hejazi and Amiji, 2003). It dissolves and swells in acidic media due to ionization of the amino groups of the CS molecules. CS has been extensively used in many fields, e.g. agriculture, water and waste treatment, food and beverages, cosmetics, and pharmaceutics (Rinaudo, 2006), due to its biodegradability, biocompatibility, and non-toxicity (Illum, 1998). In the field of pharmaceutics, CS has been used as an excipient, e.g. as film forming agent and gelling agent. Additionally, CS provides controlled-release properties to drugs and has been used in the preparation of tablets (El-Kamel et al., 2002), beads (Anal and Stevens, 2005), microspheres (Hejazi and Amiji, 2002), gels (Senel et al., 2000), and films (Remuñán-López et al., 1998; Senel et al., 2000).

Due to its positive charge, CS is able to interact with negatively charged clay, which has a silicate layer structure. When CS dispersions were mixed with clays, the zeta potential of clays and the viscosity of the composite dispersion were changed (Günister et al., 2007; Khunawattanakul et al., 2008). The dry material obtained from these composite dispersions is called nanocomposite if CS intercalates into the silicate layer of the clay (Alexandre and Dubois, 2000). Different type of clays, such as montmorillonite (Darder et al., 2003, 2005; Wang et al., 2005), magidiite (Liu et al., 2007), and rectorite (Wang et al., 2006, 2007), have all be used to prepare nanocomposite materials with CS. In the preparation process of these materials, it is necessary to use a heat treatment on the composite dispersion to induce the formation of nanocomposites (Darder et al., 2003, 2005; Wang et al., 2005). Furthermore, the clay content influenced thermal stability and mechanical properties of the nanocomposites (Wang et al., 2005). CS–clay nanocomposites were developed and characterized for use as biosensors (Fan et al., 2007; Zhao et al., 2008), packaging materials (Rhim et al., 2006), and superabsorbent materials (Ruiz-Hitzky et al., 2005). Moreover, CS–clay films could retard the release of a bioactive agent incorporated into the films (Wang et al., 2007).

* Corresponding author. Tel.: +66 43 362092; fax: +66 43 202379.
E-mail address: thaned@kku.ac.th (T. Pongjanyakul).

0378-5173/$ – see front matter © 2010 Elsevier B.V. All rights reserved.
doi:10.1016/j.ijpharm.2010.04.007

Magnesium aluminum silicate (MAS) is a purified bentonite, which has been widely used as pharmaceutical excipient, e.g. as suspending and stabilizing agent (Kibbe, 2000). MAS is a mixture of colloidal montmorillonite and saponite. It is composed of three-lattice layers with a central octahedral sheet of aluminum or magnesium and two external silica tetrahedron sheets (Alexandre and Dubois, 2000). The surface silicate layers of MAS have a negative charge, whereas the edges of the layers possess a positive charge. The positively charged edges of MAS can interact, e.g. with sodium alginate resulting in an increase in the thixotropic properties of the composite dispersions (Pongjanyakul and Puttipipatkhachorn, 2007). Sodium alginate–MAS dispersions could be used as a coating material for modified-release tablets (Pongjanyakul et al., 2005). In a previous study we have shown that MAS can also interact with CS to form flocculates, and the CS–MAS dispersion presented higher viscosity than either the CS or MAS dispersions alone. Composite dispersion pretreated at high temperatures resulted in smaller sized flocculates and a lower viscosity when compared with non-heated dispersions (Khunawattanakul et al., 2008). The change of the characteristics of the composite dispersions after heating may affect physicochemical properties and drug permeability of the films.

Therefore, the aims of the present study were to investigate the effect of MAS content and heat treatment of the CS–MAS dispersion before film casting on the physicochemical properties of the CS–MAS films. The CS–MAS films at various MAS contents were prepared using non-heated and heated dispersions, and a casting/solvent evaporation technique was used in this study to form the films. Physicochemical properties of the films obtained (such as thermal behavior, mechanical properties, nanocomposite formation, and molecular interactions between CS and MAS), were characterized. Moreover, water uptake properties in various media, and water vapor and drug permeabilities across the films were also examined.

2. Materials and methods

2.1. Materials

CS (with a molecular weight of 800 kDa and a degree of deacetylation of 85%) was purchased from Seafresh Chitosan (Lab) Co., Ltd. (Bangkok, Thailand). MAS (Veegum®HV) was obtained from R.T. Vanderbilt Company, Inc. (Norwalk, CT, USA). Propranolol HCl (PPN), diclofenac sodium (DCF) and acetaminophen (ACT) were purchased from Changzhou Yabang Pharmaceutical Co., Ltd. (Jiangsu, China), Sigma Chemical Company (MO, USA), and Praporn Darsut, Ltd. (Bangkok, Thailand), respectively. All other reagents used were of analytical grade and used as received.

2.2. Preparation of CS and CS–MAS films

CS and CS–MAS composite dispersions were prepared following the method of Khunawattanakul et al. (2008). Briefly, 1% (w/v) CS in 1% acetic acid was prepared and the CS dispersion was stirred overnight at room temperature. MAS (4%, w/v) was dispersed in hot water, then diluted with 10 mM acetate buffer at pH 4 to achieve the final concentration of 1% (w/v) MAS. The CS dispersion was mixed with various amounts of MAS dispersion to achieve CS–MASCS–MAS ratios of 1:0, 1:0.2, 1:0.6, and 1:1 by weight. The volume of the composite dispersion was finally adjusted to 200 ml with 10 mM acetate buffer at pH 4. The composite dispersions were mixed for 5 min using a homogenizer and stored at room temperature for 24 h before being poured onto a plastic plate (15 cm × 20 cm) and allowed to evaporate at 45 °C. The dry films were peeled of and kept in a desiccator. To investigate the effect of heat treatment of the composite dispersion on the physicochemical properties of the films, the CS and CS–MAS composite dispersions were prepared using the method mentioned above and incubating at 60 °C for 48 h before film casting.

2.3. Thickness of the films

Thickness of the dry and wet films was measured in ten places using a microprocessor coating thickness gauge (Minitest 600B, ElektroPhysik, Germany). The dry films were cut and placed on a control plate. The probe, which was connected to the measurement gauge and calibrated using a standard film, gently moved downward to touch the film, and the thickness of film was then measured. The films were subsequently placed in a small beaker containing deionized water or pH 6.8 phosphate buffer, which was shaken occasionally in a water bath at 37.0 ± 0.5 °C for 1 h. The samples were taken and blotted to remove excess water. The thickness of the wet films was immediately determined following the procedure mentioned above.

2.4. Surface and matrix morphology

Surface and matrix morphology of the films was observed by scanning electron microscopy (SEM). For matrix morphology studies, the films were immediately fractured after immersion in liquid nitrogen for 2 s. The films were mounted onto stubs, sputter coated with gold in a vacuum evaporator and photographed using a scanning electron microscope (JEOL Model JSM-6400, Tokyo, Japan).

2.5. Fourier transform infrared (FTIR) spectroscopy

FTIR spectra of the samples were determined using the KBr disc method. Each sample was ground and gently triturated with KBr and then pressed with a hydrostatic press at 10 tons for 15 min. The discs were placed in a sample holder and scanned from 4000 to 400 cm^{-1} at a resolution of 4 cm^{-1} (Spectrum One, Perkin Elmer, Norwalk, CT).

2.6. Nuclear magnetic resonance (NMR) spectroscopy

The ^{29}Si NMR spectra of the samples were measured using a solid-state ^{29}Si cross-polarization, magic angle spinning (CP/MAS) NMR spectrometer (DPX-300, Bruker-BioSpin AG, Fällanden, Switzerland). The spectral parameters used were as follows: 1600 spins, a relaxation delay of 6 s, and a spin rate of 5 kHz. The method validation was performed by measuring MAS powder for triplicate. The relative standard deviation of the ^{29}Si chemical shift of MAS located at −94.07 ppm was found to be 0.0139%, indicating good accuracy of this measurement.

2.7. DSC studies

Thermal behavior of the films was studied by using a differential scanning calorimeter (DSC822^e, Mettler Toledo, Switzerland). Samples (2–4 mg, accurately weighed) were placed into 40 μl aluminum pans without an aluminum cover. Measurements were performed over a temperature range from 30 to 450 °C at a heating rate of 10 °C/min.

2.8. Powder X-ray diffractometry (PXRD)

X-ray diffraction pattern of samples were recorded using a powder X-ray diffractometer (TTRAXIII, Rigaku, Malaysia) using Cu Kα radiation generated at 50 kV and 300 mA as X-ray source, an angular of 1–10° (2θ) and a step angle of 0.04° (2θ) s^{-1}. The silicate layer

thickness of MAS could be calculated using Bragg's equation:

$$n\lambda = 2d\ \sin\theta \quad (1)$$

where n is 1 (the first order reflection), λ is the wavelength of the X-ray (1.54 Å), θ is the angle of the basal spacing peak of MAS, and d is the silicate layer thickness of MAS.

2.9. Mechanical properties of films

Mechanical properties of films were measured using a Texture Analyzer (TA-XT2, Stable Micro Systems, Ltd., UK). The films were cut into 10 cm × 1 cm strips, and kept in a humidity controlled chamber (55%RH, 25 °C) for 3 days before testing (ASTM, 2002; Pongjanyakul et al., 2005). The measurements were performed using a 5-kg loaded cell, a gauge length of 5 cm, and a cross-head speed of 0.2 mm/s. The stress used was plotted against strain to obtain stress–strain curves. The tensile strength and percentage of elongation at break of the films are reported.

2.10. Water uptake studies

Water uptake studies of the films were carried out using a gravimetric method. Films were soaked in deionized water or pH 6.8 phosphate buffer and shaken occasionally at 37.0 ± 0.5 °C. After a predetermined time interval, each film was withdrawn, blotted to remove excess water, immediately weighed (W_t), and then dried in a hot air oven at 50 °C to a constant weight (W_d). The percent water uptake can be calculated from the following equation (Ritthidej et al., 2002; Tuovinen et al., 2003):

$$\text{Water uptake}(\%) = \left(\frac{W_t - W_d}{W_d}\right) \times 100 \quad (2)$$

2.11. Water vapor permeability studies

Water vapor permeability of the films was investigated following the method of Remuñán-López and Bodmeier (1997). The films were cut into a disc shape with a diameter of 1 cm, placed on open glass vials containing silica gel beads and held in place with a screw lid with a 0.61-cm^2 test area. The vials were placed in a desiccator kept at 25 ± 1 °C and containing a saturated aqueous sodium chloride solution (75% RH). The weight gain of the vials, i.e. the amount of water vapor permeated through the films, was periodically recorded over 72 h. The amount of water vapor permeated per area was plotted against time and the slope of this relationship was the water vapor permeation (WVP) rate. The WVP coefficients of the films were calculated using the following equation (Pongjanyakul et al., 2005):

$$\text{WVP coefficient} = \frac{Mh}{A\ \Delta P_v} \quad (3)$$

where M is the WVP rate, h is the film thickness, A is the area of the exposed films, and ΔP_v is the vapor pressure difference.

2.12. Drug permeability studies

Drug permeability studies were performed using a side-by-side diffusion cell (Crown Glass Co., Inc., Somerville, NJ) at 37.0 ± 0.5 °C. Deionized water or pH 6.8 phosphate buffer were used as release media in this study. The films were hydrated in medium for 1 h and then clamped between donor and receptor compartments with a 3 ml volume and a diffusion area of 0.67 cm^2. Drug solution at a concentration of 4 mg ml^{-1} was placed in the donor phase, while the receptor phase compartment contained 3 ml of medium. Both compartments were continuously stirred throughout the tests. At predetermined intervals, 2.6 ml of medium in the receptor compartment was collected and replaced with an equal volume of fresh medium. Acetaminophen (ACT), diclofenac sodium (DCF) and propranolol hydrochloride (PPN) were selected as model drugs to study the effect of different drug types on film permeability. The amount of ACT, DCF and PPN in the collected samples was measured by UV spectroscopy (Shimadzu UV1201, Japan) at a wavelength of 265, 260 and 289 nm, respectively.

Drug permeation through the films was determined under steady state conditions by means of Fick's first law (Flynn et al., 1974; Sinko, 2006), which can be expressed as:

$$\frac{dQ}{A\ dt} = PC_0 \quad (4)$$

where $dQ/A\,dt$ is the permeation flux (the slope calculated using linear regression analysis of the relationship between the amount of drug permeated per surface area of the films (A) and time). C_0 is the concentration of drug in the donor compartment and P is permeability coefficient. The apparent diffusion coefficient (D) was estimated from the following equation:

$$t_L = \frac{h^2}{6D} \quad (5)$$

where t_L is the lag time, obtained from the x-intercept of the permeation profiles, and h is the mean thickness of the wet films.

2.13. Statistical analysis

One-way analysis of variance (ANOVA) with the least significant difference (LSD) test for multiple comparisons and Student's t-test were used to compare the different results of tensile strength, %elongation, WVP coefficient and drug permeation parameters of the films. All statistical tests were performed using the software SPSS for MS Windows, release 11.5 (SPSS (Thailand) Co., Ltd., Bangkok, Thailand). The significance of the difference was determined at 95% confident limit ($\alpha = 0.5$) and considered to be significant at a level of P less than 0.05.

3. Results and discussion

3.1. Morphology and thickness of the films

All of the films were successfully prepared using the casting/solvent evaporation method. CS films obtained were transparent and yellowish, whereas addition of MAS resulted in an opaque appearance of the CS–MAS films. The microscopic surface and matrix morphology of the films using various CS–MAS ratios are shown in Fig. 1a–d. While a smooth surface of the CS films was found, increasingly rougher surfaces were observed when increasing the MAS content in the films. The matrix morphology of the films changed from a dense matrix of the CS films to a layer structure of the CS–MAS films. The CS–MAS (1:1) film prepared using a non-heated dispersion showed the similar surface morphology and matrix structure than that prepared using a heated dispersion (Fig. 1d and e, respectively).

The dry thickness of the films increased with increasing content of MAS (Table 1). This was due to an increase of solid content in the same dispersion volume for film casting. The wet thicknesses of the films hydrated in deionized water and pH 6.8 phosphate buffer were significantly higher than the dry thicknesses of the films (Table 1), indicating swelling properties of the films. The %thickness increase after hydration of the films prepared using non-heated dispersion in deionized water increased when increasing of MAS content, whereas the films prepared using heated dispersion gave lower %thickness increase after hydration than those prepared using non-heated dispersions. This suggests that heat treatment caused a decrease of swelling properties of the films. Moreover, an obvious decrease of %thickness increase after hydra-

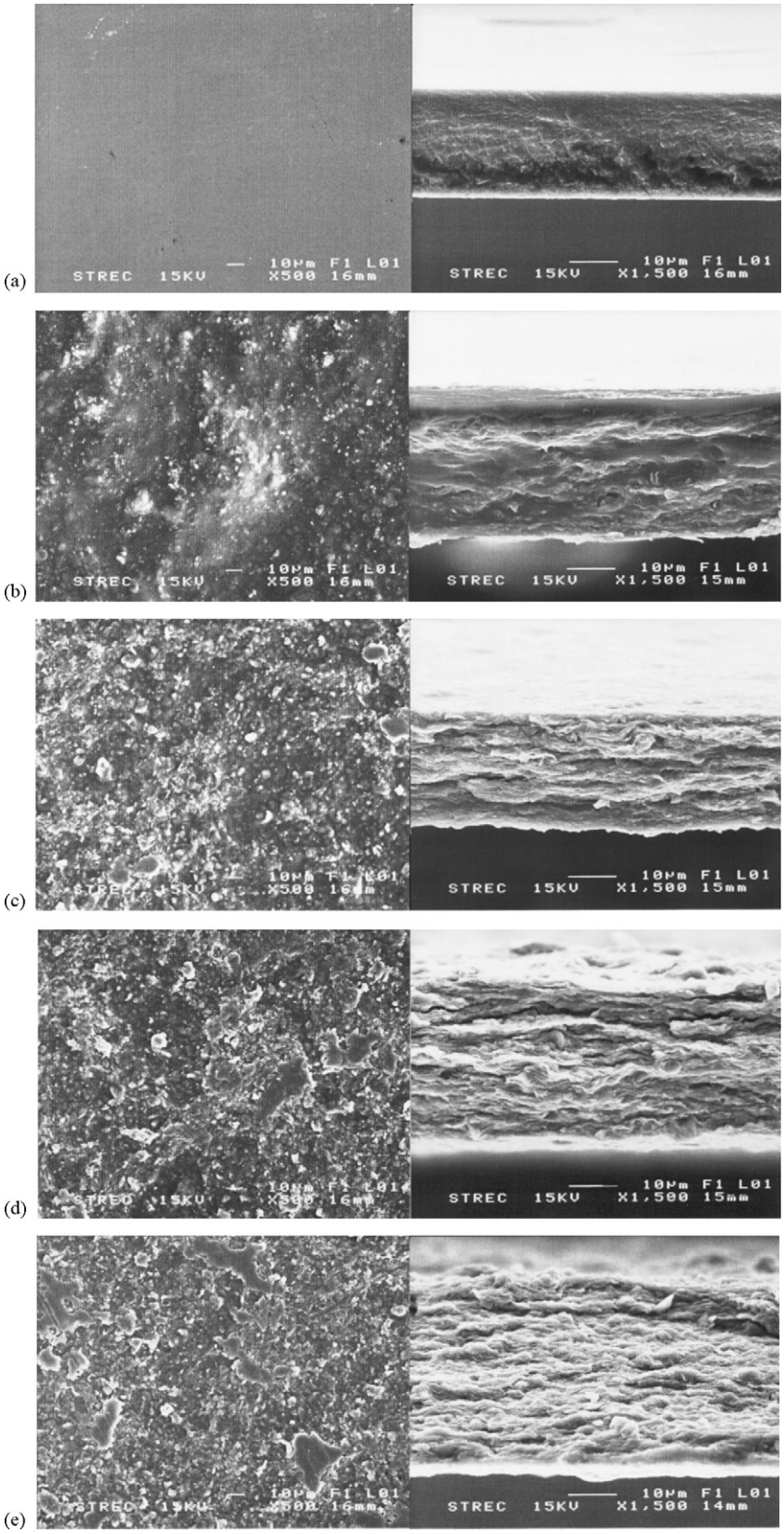

Fig. 1. Surface and matrix morphology of CS film (a), CS–MAS film at the ratios of 1:0.2 (b), 1:0.6 (c) and 1:1 (d) prepared using non-heated dispersions, and CS–MAS (1:1) films (e) prepared using a heated dispersion.

Table 1
Thickness and water uptake of CS–MAS films in different media.

CS–MAS ratio (by weight)	Dry thickness[a] (μm)	Wet thickness[a] (μm)		Water uptake[b] (%)	
		Deionized water	pH 6.8 phosphate buffer	Deionized water	pH 6.8 phosphate buffer
Non-heated dispersion					
1:0	24.7 ± 1.3	53.0 ± 2.8 (114.6%)	48.6 ± 2.2 (96.8%)	216.9 ± 11.0	106.6 ± 12.4
1:0.2	33.2 ± 3.4	85.1 ± 8.4 (156.3%)	63.9 ± 11.5 (92.5%)	550.6 ± 12.9	141.7 ± 24.9
1:0.6	42.8 ± 3.4	112.4 ± 10.2 (162.6%)	67.3 ± 5.7 (57.2%)	158.6 ± 10.4	75.8 ± 7.1
1:1	50.0 ± 4.3	144.1 ± 14.4 (188.2%)	63.9 ± 5.4 (27.8%)	141.8 ± 17.2	80.5 ± 15.4
Heated dispersion					
1:0	39.9 ± 2.9	88.2 ± 5.9 (121.1%)	47.1 ± 11.7 (18.0%)	257.3 ± 96.0	63.5 ± 14.5
1:0.2	45.7 ± 5.6	90.0 ± 13.7 (96.9%)	74.4 ± 8.9 (62.8%)	614.6 ± 82.6	151.2 ± 12.6
1:0.6	42.3 ± 4.0	99.2 ± 15.1 (134.5%)	67.2 ± 7.7 (58.9%)	102.5 ± 22.6	59.8 ± 12.7
1:1	54.0 ± 2.7	126.5 ± 8.1 (134.3%)	59.7 ± 6.8 (10.6%)	125.6 ± 4.6	90.8 ± 5.0

Thickness increase after hydration (%) is shown in parentheses and calculated using the equation: ((mean wet thickness − mean dry thickness)/mean dry thickness) × 100.
[a] Data are the mean ± S.D., $n = 10$.
[b] Data are the mean ± S.D., $n = 4$.

tion of the films was found in pH 6.8 phosphate buffer when compared with deionized water. It can be explained by CS being cross-linked by phosphate anions (Nunthanid et al., 2001), resulting in a lower hydration of the CS and CS–MAS films in pH 6.8 phosphate buffer.

3.2. Molecular interaction between CS and MAS

The FTIR spectrum of CS powder showed the OH stretching peak, which overlapped with the NH stretching, at 3372 cm^{-1} and the CH stretching peak around 2877–2922 cm^{-1}. The carbonyl stretching (amide I) peak, NH_2 bending (amide II) peak of primary amine and CH_2 bending peak were found at 1650, 1599 and 1422 cm^{-1}, respectively (Fig. 2b). The appearance of the carbonyl stretching peak suggested the structure of N-acetylglucosamine, indicating that this CS grade used was not absolutely deacetylated (Nunthanid et al., 2001). The FTIR spectra of CS films showed a shift of the NH_2 bending peak to a lower wavenumber (1567 cm^{-1}) as presented in Fig. 2c, suggesting an interaction of protonated primary amine with acetic acid that used as a solvent, indicative of a formation of chitosonium acetate (Puttipipatkhachorn et al., 2001; Kasaai, 2008). Moreover, the CH_2 bending peak was also moved to a lower wavenumber. This may be due to hydrogen bonding formation between the primary hydroxyl groups and acetic acid, and rearrangement of hydrogen bonds of the primary hydroxyl groups of polysaccharides (Harish Prashanth et al., 2002; Kasaai, 2008). Heat treatment of the CS dispersions did not influence the FTIR spectra of the CS films (Fig. 2d). The CS–MAS films prepared using both heated and non-heated dispersions displayed similar spectra. A lower wavenumber shift of the NH_2 bending peak of the CS films was found when adding MAS (Fig. 2e), indicating the electrostatic interaction between the negatively charged MAS and the protonated amine groups of CS. Furthermore, the SiOH stretching peak of MAS at 3632 cm^{-1} (Fig. 2a) was moved to 3611–3615 cm^{-1} and a shift of the CH stretching and the CH_2 bending peaks of CS were also found when adding MAS (Fig. 2e and f). This suggests that the silanol groups on the surface of the MAS silicate layers could form an intermolecular hydrogen bond with CS. Interestingly, the CS–MAS films prepared using both heated and non-heated dispersions presented a new peak at around 3682 cm^{-1}. This absorption peak represented the stretching of free SiOH groups (Kamiya et al., 2000; Patel et al., 2007) when the thickness of the silicate layers was increased, and was not found in MAS powder. This may suggest that CS can be intercalated into the silicate layer of MAS and will be discussed later in the PXRD studies.

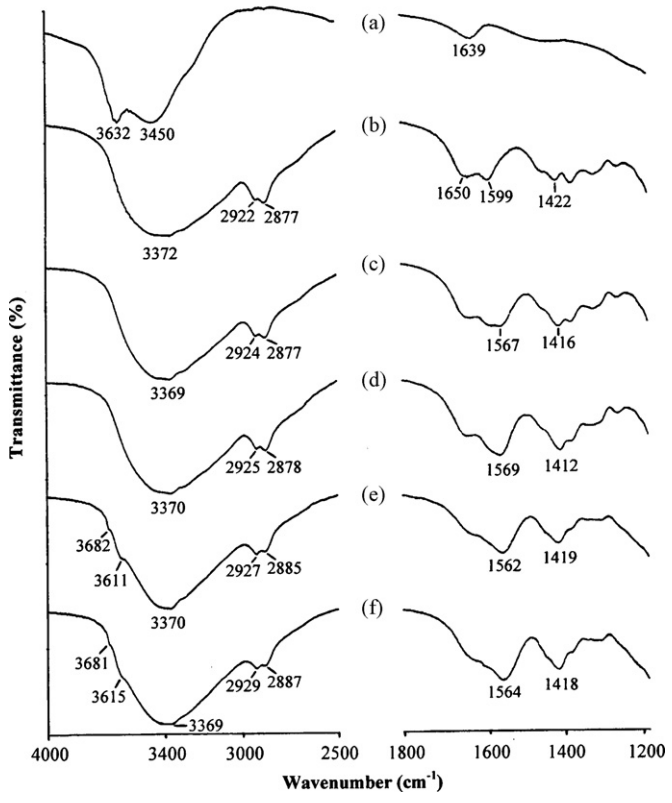

Fig. 2. FTIR spectra of MAS powder (a), CS powder (b), CS films prepared using non-heated (c) and heated (d) dispersions, and CS–MAS (1:1) films prepared using non-heated (e) and heated (f) dispersions.

The solid-state ^{29}Si NMR spectra of the CS–MAS films are shown in Fig. 3. The ^{29}Si NMR spectra give evidence of electronic changes in the tetrahedral sheet of montmorillonite. The slightly negative change in the ^{29}Si chemical shift indicates a decrease in the charge of the montmorillonite silicate layers (Gates et al., 2000). In this study, the ^{29}Si chemical shift of MAS was located at −94.07 ppm (Fig. 3a). The signal of this chemical shift displayed stronger intensities with increasing MAS content in the films. A slightly negative change in the chemical shift of the CS–MAS films was observed (Fig. 3b–d). Moreover, an increase in negative change of this chemical shift of the CS–MAS films prepared using a heated dispersion was found compared with those prepared using non-heated dispersions. These results were similar to the previous studies where MAS interacted with amine drugs to form complexes (Pongjanyakul et al., 2009; Rojtanatanya and Pongjanyakul, 2010). This finding indicates that the negative charge on the MAS silicate layers electrostatically interacted with the protonated amine groups of CS.

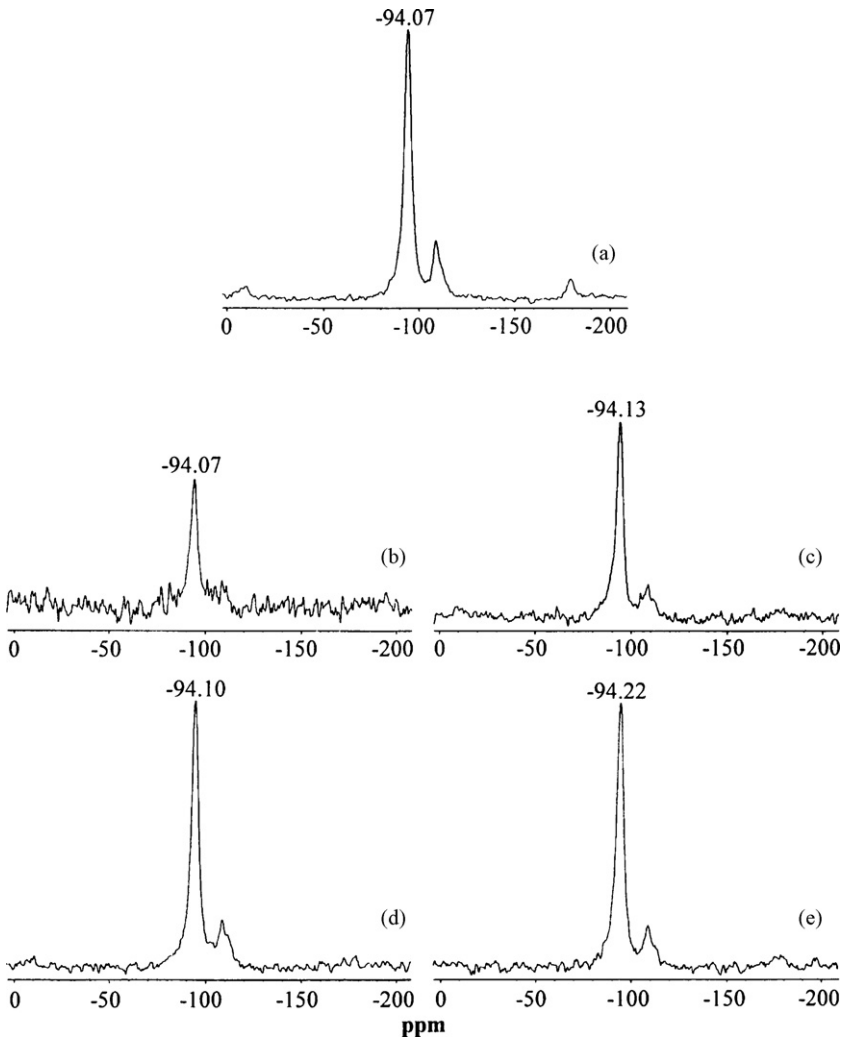

Fig. 3. Solid-state ^{29}Si NMR spectra of MAS powder (a), CS–MAS films in the ratios of 1:0.2 (b), 1:0.6 (c), and 1:1 (d) prepared using non-heated dispersions, and CS–MAS (1:1) films (e) prepared using a heated dispersion.

3.3. PXRD studies

The nanocomposite formation between CS and MAS in the films was investigated using PXRD. MAS powder showed a diffraction peak at 6.5° (2θ) (Fig. 4a), indicating the basal spacing peak and a thickness of the MAS silicate layer of 1.37 nm. The CS–MAS (1:0.2) films prepared using non-heat and heated dispersions had no obvious basal spacing peak of MAS as shown in Fig. 4c and g, respectively. This suggests the formation of exofoliated nanocomposite films due to a complete separation of the MAS silicate layers in the CS matrix (Alexandre and Dubois, 2000). This type of nanocomposite can be formed because a low content of MAS was dispersed in the films (Ray and Okamoto, 2003). The basal spacing peak of MAS clearly appeared at 4.5 and 4.4° (2θ) for the CS–MAS films at the ratios of 1:0.6 and 1:1 prepared using non-heated dispersions, respectively, resulting in an increased thickness of the MAS silicate layers of 1.96 and 2.01 nm, respectively. This indicates the formation of intercalated nanocomposites in which CS could intercalate into the MAS silicate layers. The CS–MAS (1:0.6) films prepared using a heated dispersion also showed the basal spacing peak of MAS (at 6.1° (2θ), Fig. 4h), again suggesting the formation of an intercalated nanocomposite. Additionally, multiple layers of CS could intercalate into the MAS silicate layers as evidenced by the peaks at 2.2 and 4.3° (2θ) of the films prepared at the ratio of 1:1 using heated dispersion, leading to the highest thickness of the MAS silicate layers in this study (4.1 nm). Darder et al. (2005) reported that bilayered CS could intercalate into montmorillonite and a thickness of the silicate layers of 2.04 nm was found. This suggests that in the current study more than two layers of CS molecules could be intercalated into the MAS silicate layers. The findings presented here indicate that for a nanocomposite formation between CS and MAS it was not necessary to use the heat treatment to the composite dispersions before film casting, but the heat treatment resulted in the formation of nanocomposites that could induce multilayers of CS intercalated into the MAS silicate layers when using the 1:1 ratio of CS and MAS.

3.4. Thermal analysis

The DSC thermogram of CS powder presented a broad endothermic peak at around 45–60 °C and an exothermic peak at 306 °C, indicating water residue evaporation and decomposition of CS, respectively (Fig. 5a). The exothermic decomposition peak of CS films shifted to a lower temperature at around 287 °C (Table 2) with a lower decomposition enthalpy (Fig. 5c). This result is in agreement with previous reports (Nunthanid et al., 2001; Ritthidej et al., 2002) and is due to the formation of chitosonium acetate in the films using acetic aqueous solution as a solvent, leading to an amorphous and partial crystalline state of CS films when compared with crystalline CS powders (Nunthanid et al., 2001). Moreover, residue

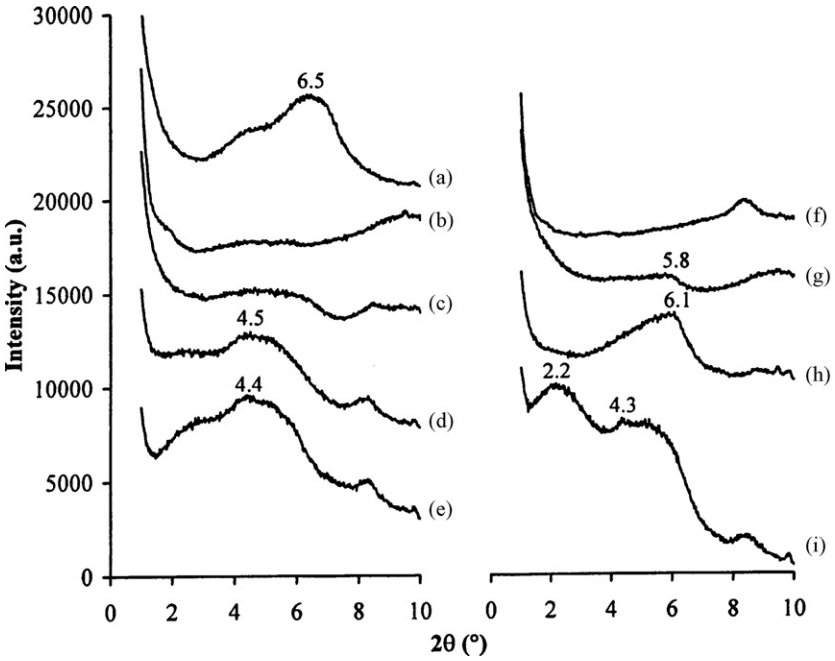

Fig. 4. XRD pattern of MAS powder (a), CS film (b) and CS–MAS films in the ratios of 1:0.2 (c), 1:0.6 (d), and 1:1 (e) prepared using non-heated dispersions, and CS film (f) and CS–MAS films in the ratios of 1:0.2 (g), 1:0.6 (h) and 1:1 (i) prepared using heated dispersions.

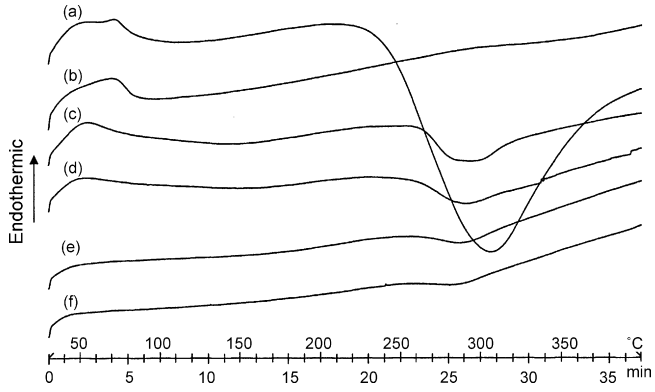

Fig. 5. DSC thermograms of CS powder (a), MAS powder (b), CS film (c), and CS–MAS films in the ratios of 1:0.2 (d), 1:0.6 (e), and 1:1 (f) prepared using non-heated dispersions.

acetic acid in the films induced thermal degradation of CS at lower temperatures (Wang et al., 2005). Addition of MAS into the CS films caused a decrease in exothermic peak intensity and the decomposition temperature of CS did not obviously change (Table 2 and Fig. 5d–f). The CS films prepared using a heated dispersion showed an exothermic decomposition peak at 270 °C (Table 2), which was lower than for CS films prepared using non-heated dispersions. It has been described that heat treatment causes a reduction of intramolecular hydrogen bonding of CS (Chen and Tsaih, 1998) and also may induce thermal depolymerization of CS (Holme et al., 2008), resulting in a decrease of viscosity of CS dispersions after heat treatment (Khunawattanakul et al., 2008). This may also have led to a lower thermal stability of the CS films. Surprisingly, incorporation of MAS caused an increase in decomposition temperature of CS in the composite films prepared using heated dispersions (Table 2). This suggests that the interaction of CS with MAS by flocculation in the composite dispersion and the intercalation of CS into the MAS silicate layers could possibly protect the CS molecules from the thermal depolymerization when treated by heating. Therefore, the formation of intercalated nanocomposites could improve the thermal stability of the CS–MAS films.

Table 2
Degradation peak temperature of CS in CS–MAS films prepared using non-heated and heated dispersions.

CS–MAS ratio (by weight)	Exothermic peak temperature (°C)	
	Non-heated dispersion	Heated dispersion
1:0	286.8	269.7
1:0.2	292.2	278.7
1:0.6	287.9	286.4
1:1	286.0	283.0

3.5. Mechanical properties studies

The mechanical properties of the films, tensile strength and %elongation, are presented in Fig. 6. The tensile strength of the CS films prepared using non-heated dispersions significantly decreased ($P < 0.05$) with adding 0.2 g of MAS, whereas the tensile strengths of the CS–MAS films in the ratios of 1:0.6 and 1:1 were comparable and had a higher tensile strength than the CS films. The CS films and the CS–MAS films prepared using heated dispersions provided statistically greater tensile strength ($P < 0.05$) than those prepared using non-heated dispersions, except when the 1:0.6 ratio of CS–MAS was used. The %elongation of all CS–MAS films was higher than for the CS films, with the CS–MAS films in the ratios of 1:0.2 and 1:0.6 having a remarkably higher %elongation ($P < 0.05$) than that of the 1:1 ratio film. Moreover, heat treatment significantly decreased %elongation ($P < 0.05$) of the CS–MAS films in the ratios of 1:0.2 and 1:0.6, but the highest %elongation was found in the films with 1:1 ratio.

Heat treatment applied to the dispersions before film casting overall increased the tensile strength, but reduced the elongation of the CS films. This is likely to be due to the depolymerization of CS chains, with the shorter CS chains forming a denser matrix film during the drying process. This led to a high strength of the films but also caused a decrease of the flexibility of the films. The exfoliated nanocomposite structure of the CS–MAS (1:0.2) films decreased the tensile strength of the CS film because the MAS interacted with CS and dispersed completely in the CS matrix interrupting the

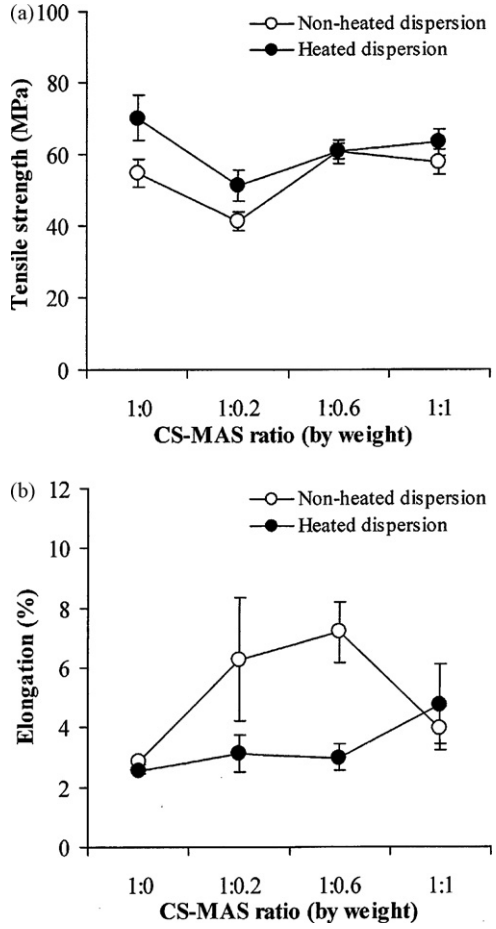

Fig. 6. Tensile strength and %elongation of CS and CS–MAS films at various ratios of CS and MAS prepared using non-heated and heated dispersions. Each value is the mean ± S.D., $n = 5$.

intermolecular hydrogen bonding of CS. However, the higher MAS content of the CS–MAS films gave higher tensile strength than the CS films, suggesting that the intercalation of CS into the MAS silicate layers could create the strong matrix structure of the films and the heat treatment did not affect the matrix formation. Moreover, the exfoliated and intercalated nanocomposite of the CS–MAS films in the ratios of 1:0.2 and 1:0.6 gave obviously higher %elongation than the CS films. The increased elongation of these films may be due to the formation of dangling chains and conformational effects at the clay–matrix interface (Alexandre and Dubois, 2000). However, the highest content of MAS in the films decreased the %elongation of the nanocomposite films. This result was in agreement with a previous study (Wang et al., 2007). This phenomenon could generally occur in the films loaded with solid particles even if the solid particles did not interact with the polymers (Okhamafe and York, 1984; Felton and McGinity, 2002). On the other hand, the CS–MAS (1:1) film prepared using heated dispersions provided the highest %elongation when compared with those prepared using the same method. This suggests that the formation of CS multilayers intercalated into the MAS silicate layer could possibly enhance the flexibility of the films. Furthermore, the layer matrix structure of the CS–MAS nanocomposite films observed using SEM could generally improve the %elongation of the films and also give the strength of the films.

3.6. Water uptake studies

Water uptake of the films in deionized water and pH 6.8 phosphate buffer is shown in Table 1. Incorporation of MAS caused a decrease in water uptake of the films in deionized water, except for the CS–MAS (1:0.2) films which showed the highest water uptake. This result is in contrast to the study of Wang et al. (2007), who reported that the nanocomposite film of CS and rectorite, which has a similar structure and characteristics to montmorillonite, showed a continuous decrease of water uptake with increasing rectorite ratio in the films. This suggests that the interaction of CS with MAS to create the intercalated nanocomposite gave a denser matrix structure with smaller water-filled channels. However, the exfoliated nanocomposite of the CS–MAS (1:0.2) films could highly absorb water when compared with the intercalated nanocomposites. This may be due to the completely dispersed MAS in the CS matrix, leading to higher water uptake efficiency. This may also suggest the presence of larger water-filled channels in this film. The CS–MAS films in the ratios of 1:0.6 and 1:1 prepared using heated dispersions gave lower water uptake than those prepared using non-heated dispersions. In contrast, the CS and CS–MAS (1:0.2) films prepared using heated dispersion showed higher water uptake than those prepared using non-heated dispersion. The shorter chains of CS, because of the depolymerization of CS at high temperature, may have caused the formation of larger water-filler channels in the films. This suggests that the heat treatment affected the water uptake and swelling properties in deionized water as was partially discussed in Section 3.1. Additionally, an obviously lower water uptake of the films in pH 6.8 phosphate buffer was observed when compared with using deionized water because CS could be cross-linked by phosphate anions (Nunthanid et al., 2001). The anions cross-linked CS resulted in denser matrix structures and restricted water penetration into the films.

3.7. Water vapor permeability studies

Incorporation of MAS into the CS films could retard the WVP rate of the films prepared using heated and non-heated dispersions, most likely due to the increase in film thickness when adding MAS. The WVP coefficient calculated using Eq. (3) was used for comparison as shown in Fig. 7. It can be observed that the CS–MAS (1:0.2) films gave slightly higher WVP coefficient than the CS films and the CS–MAS films with higher content of MAS. This suggested that the exfoliated nanocomposite films had a looser matrix structure and water vapor could more easily permeate through the films. The increase in MAS ratio in the CS–MAS films did not lead to different WVP coefficients when compared with the CS films.These results

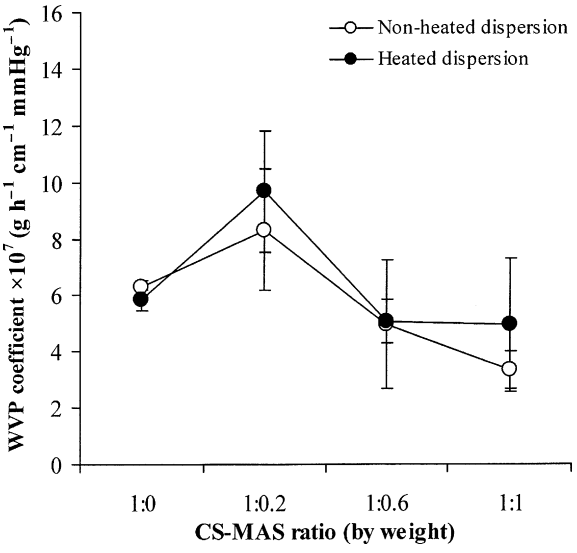

Fig. 7. Water vapor permeation (WVP) coefficient of CS and CS–MAS films at various ratios prepared using non-heated and heated dispersions. Each value is the mean ± S.D., $n = 4$.

Table 3
Permeation parameters of PPN through CS and CS–MAS films.

CS–MAS ratio (by weight)	Deionized water			pH 6.8 phosphate buffer		
	$P \times 10^5$ (cm^2 s^{-1})	Lag time (min)	$D \times 10^8$ (cm^2 s^{-1})	$P \times 10^5$ (cm s^{-1})	Lag time (min)	$D \times 10^8$ (cm^2 s^{-1})
Non-heated dispersion						
1:0	3.01 ± 0.24	0.77 ± 0.05	10.20 ± 0.66	5.55 ± 0.34	0.89 ± 0.24	7.71 ± 1.80
1:0.2	3.38 ± 0.20	6.36 ± 0.79	3.19 ± 0.38	6.48 ± 0.69	2.05 ± 0.78	6.05 ± 2.09
1:0.6	1.45 ± 0.10	12.57 ± 2.24	2.87 ± 0.47	3.75 ± 0.06	5.83 ± 0.14	2.16 ± 0.05
1:1	1.39 ± 0.05	22.52 ± 1.23	2.57 ± 0.14	0.75 ± 0.10	47.93 ± 2.20	0.24 ± 0.01
Heated dispersions						
1:0	2.94 ± 0.14	0.52 ± 0.04	41.87 ± 3.58	6.73 ± 0.35	0.39 ± 0.05	15.95 ± 2.23
1:0.2	4.11 ± 0.65	3.09 ± 0.41	7.37 ± 0.91	6.55 ± 0.62	1.21 ± 0.39	13.48 ± 3.66
1:0.6	0.83 ± 0.05	28.59 ± 2.32	0.96 ± 0.08	3.88 ± 0.12	3.36 ± 0.15	3.74 ± 0.16
1:1	1.03 ± 0.07	27.69 ± 4.64	1.63 ± 0.25	0.89 ± 0.05	30.25 ± 6.30	0.34 ± 0.07

Data are the mean ± S.D., $n = 3$.

are in contrast to the WVP characteristics of the CS-rectorite films, where rectorite retarded the water vapor permeation (Wang et al., 2007). This may be due to the high content of MAS used in this study, which may affect matrix structure formation. On the other hand, sodium alginate–MAS microcomposite films gave higher WVP coefficients when increasing MAS content because the higher content of MAS may cause a formation of small channels in the film matrix structure (Pongjanyakul et al., 2005). This indicated that the intercalated nanocomposites formed at higher content of MAS gave a denser matrix structure of the film. Moreover, the heat treatment did not influence the water vapor permeability of the films. This may be due to water being a very small molecule that could rapidly diffuse through the films.

3.8. Drug permeability studies

Cumulative PPN permeation profiles across the films using deionized water and pH 6.8 phosphate buffer were linear ($R^2 > 0.98$) with a lag time. This indicated that the PPN permeation reached a steady state and could be described using Fick's first law. The PPN permeation parameters using deionized water are presented in Table 3. It can be seen that a significantly longer lag time ($P < 0.05$) was found when increasing MAS content in the CS films. The increased MAS concentration caused a decrease in P values, except for the CS–MAS (1:0.2) films that had statistically higher P values ($P < 0.05$) than the CS films. These results were also found in the films prepared using heated dispersions. The D values computed using Eq. (5), using the wet thickness in Table 1, showed that the CS films possessed the highest D value and this value tended to decrease with increasing MAS content in the films. The D values of the CS film and the CS–MAS (1:0.2) film prepared using heated dispersion were significantly higher ($P < 0.05$) than those prepared using non-heated dispersions. In contrast, the higher MAS ratio caused a statistically lower D value ($P < 0.05$) in the CS–MAS films prepared using heated dispersion when compared with the films prepared using non-heated dispersions.

PPN has a pK_a value of 9.5 (Dollery, 1991) and the pH of the PPN solution in the donor compartment was 6.3. This means that the amine group of PPN was protonated and could interact with a negatively charged MAS (Sánchez-Martin et al., 1981; Rojtanatanya and Pongjanyakul, 2010), resulting in a high affinity of PPN with the CS–MAS films. This led to an increased lag time when increasing MAS content in the films. Moreover, the CS–MAS nanocomposite formation brought about smaller water-filled channels with higher tortuosity of the films, which could be observed from the decreasing water uptake when the MAS content increased (Table 1). Thus, lower P and D values were obtained. The CS–MAS (1:0.2) films showed higher a P value than the CS films due to the highest water uptake properties. However, the D value of the CS–MAS (1:0.2) films was lower than the CS films, indicating that the CS–MAS (1:0.2) films had a higher affinity to the drug than the CS films, even thought it had a greater water uptake. The D values of the CS film and the CS–MAS (1:0.2) film prepared using heated dispersion were higher that those prepared using non-heated dispersions. This was due to the greater water uptake of the films prepared using heated dispersions (Table 1), leading to larger water-filler channels with lower tortuosity in the wet state of the films. On the other hand, the higher MAS ratio in the CS films could form intercalated nanocomposites and the films casted using the heated dispersions had lower water uptake, suggesting smaller water-filled channels. Thus, a longer lag time and a lower D value were obtained.

Using pH 6.8 phosphate buffer, higher P values of PPN in the CS films and the CS–MAS films at the ratios of 1:0.2 and 1:0.6 were found when compared with those using deionized water. This is likely to be due to a cross-linking of CS with phosphate ions that resulted in a lower wet thickness (Table 1). Moreover, the MAS in the CS films could adsorb the positively charged sodium ion in pH 6.8 phosphate buffer, which led to a lower affinity on PPN. In contrast, the CS films with the highest MAS content showed the lowest P value and the longest lag time of PPN in pH 6.8 phosphate buffer (Table 3). This suggests that the highest MAS content had sufficient adsorption sites for PPN molecules, leading to the longest lag time of PPN permeation. The D value of PPN in the CS films using pH 6.8 phosphate buffer seemed to decrease when compared with using deionized water because the phosphate cross-linked CS films showed lower water uptake, indicating the presence of smaller water-filled channels of the films. On the other hand, the CS–MAS (1:0.2) films in pH 6.8 phosphate buffer showed higher D values than those in deionized water. It is possible that the cross-linking of CS caused the formation of many channels in an area where the MAS is dispersed in the CS films. This may have led to an increase in water uptake (Table 1), but possibly reduced tortuosity of the wet films. However, the highest MAS content in the CS films caused a significantly lower D values ($P < 0.05$) in pH 6.8 phosphate buffer. This may be due to the dense matrix structure of the films after the CS that interacted in the MAS silicate layers and was cross-linked with phosphate ions.

The effect of drug types on permeability of the CS and CS–MAS (1:0.6) films prepared using non-heated dispersions was investigated in deionized water using ACT (MW = 151.2), a non-electrolyte drug (Nakano et al., 1984; Terzyk et al., 2003), DCF (MW in free acid form = 296.1), a negatively charged drug, and PPN (MW in free base form = 259.3), a positively charged drug. The permeation parameters of the three drugs are presented in Fig. 8. The lag time of ACT was shorter than that of DCF, but the CS and CS–MAS films gave a comparable lag time for both drugs. PPN presented the longest lag time in the CS–MAS films. The P values of the CS films were higher than those of the CS–MAS films. This was due to the higher

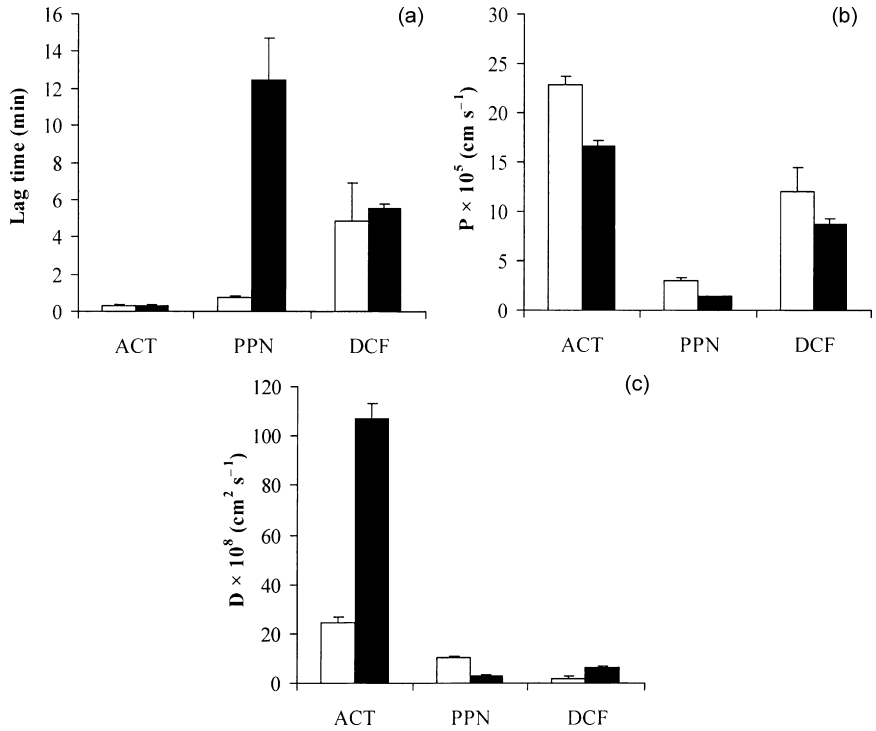

Fig. 8. Lag time (a), permeability coefficient (b), and diffusion coefficient (c) of various drugs across CS–MAS films at ratios of 1:0 (open bars) and 1:0.6 (closed bars) using deionized water as a medium. Each value is the mean ± S.D., $n = 3$.

wet thickness of the CS–MAS films, as the *P* values were inversely proportional to the membrane thickness (Sinko, 2006). The non-electrolyte ACT showed the greatest *P* value, whereas DCF provided a higher *P* value than PPN. The *D* value of ACT and DCF in the CS–MAS film was greater than that in the CS films. In contrast, PPN in the CS–MAS films gave a lower *D* value than in the CS films. The highest *D* value in this study was found for ACT.

For CS films it can be seen that the higher the molecular weight of drug, the lower the *D* value obtained. The *D* values were ordered as follows: ACT > PPN > DCF, suggesting that drug permeation across the CS film progressed via diffusion through water-filled channels, with increasing molecular weight of drug resulting in slower diffusion (Flynn et al., 1974; Pongjanyakul, 2009). In contrast, for the CS–MAS films, PPN gave a lower *D* value than ACT and DCF. This is likely to be due to ionic interaction of PPN with MAS, resulting in a longer lag time and a slower diffusion. However, it is interesting that the *D* value of ACT and DCF in the CS–MAS films was greater than those in the CS films, although a higher water uptake of the CS film was found. This suggests that the permeation mechanism across the CS–MAS films of the positively charged drug was different to the non-electrolyte and the negatively charged drugs. For positively charged drugs, the first step is the adsorption (partition) of the drug onto the MAS particles in the CS–MAS films, followed by a diffusion process in the CS fraction across the films (Pongjanyakul, 2009). In contrast, diffusion through pores could be used to describe the permeation of the non-electrolyte and the negatively charged drug. The drug is presumed to diffuse through microchannels within the structure of the hydrated CS–MAS films (Thacharodi and Panduranga Rao, 1993; Sriamornsak and Kennedy, 2008). Thus, as the nanocomposite formation of the CS–MAS films changes the CS polymer network of the matrix structure, this may result in a decrease in tortuousity of the films, leading to higher *D* values of ACT and DCF in the CS–MAS films when compared with the CS films.

4. Conclusion

This study demonstrated that the physicochemical properties of CS–MAS films depend on the MAS content and the heat treatment of the dispersion before film casting. CS can interact with MAS via electrostatic interaction and intermolecular hydrogen bonding, resulting in nanocomposite formation. For this to occur in principle, it is not necessary to apply a heat treatment to the composite dispersions. The films with low MAS content showed formation of an exfoliated nanocomposite, but multilayer CS could be intercalated into the MAS silicate layers when using higher MAS concentrations. The CS–MAS nanocomposite films prepared using non-heated dispersions provided higher %elongation than those prepared using heated dispersions. The CS–MAS films with higher MAS content and prepared using heat treatment showed a lower water uptake, resulting in lower drug permeability. The permeation mechanism of the non-electrolyte and negatively charged drugs across the CS–MAS nanocomposite films was predominantly controlled by diffusion through water-filled microchannels, whereas both adsorption onto MAS and diffusion processes occurred concurrently for the film permeation of the positively charged drugs. This finding suggest that CS–MAS nanocomposite films can be formed without the heat treatment to the composite dispersion before casting and this film could offer potential in the development for modulating drug release from coated tablets.

Acknowledgements

The authors wish to thank the Research, Development and Engineering (RD&E) Fund through the National Nanotechnology Center (NANOTEC), National Science and Technology Development Agency (NSTDA), Thailand (Project No. NN-B-22-EN4-13-50-11) for research funding and the Faculty of Pharmaceutical Sciences, Khon Kaen Univeristy, Khon Kaen, Thailand for technical support. Finan-

cial support from the Thailand Research Fund through the Royal Golden Jubilee Ph.D. Program (Grant No. PHD/0011/2549) for W. Khunawattanakul and T. Pongjanyakul is gratefully acknowledged.

References

Alexandre, M., Dubois, P., 2000. Polymer-layered silicate nanocomposites: preparation, properties and uses of a new class of materials. Mater. Sci. Eng. 28, 1–63.

American Society for Testing Material (ASTM) D882, 2002. Standard test methods for tensile properties of thin plastic sheeting. Annual Book of ASTM Standards, vol.06.01. ASTM International, West Conshohocken, pp. 164–173.

Anal, A.K., Stevens, W.F., 2005. Chitosan–alginate multilayer beads for controlled release of ampicillin. Int. J. Pharm. 290, 45–54.

Chen, R.H., Tsaih, M.L., 1998. Effect of temperature on the intrinsic viscosity and conformation of chitosans in dilute HCl solution. Int. J. Biol. Macromol. 23, 135–141.

Darder, M., Colilla, M., Ruiz-Hitzky, E., 2005. Chitosan–clay nanocomposites: application as electrochemical sensors. Appl. Clay Sci. 28, 199–208.

Darder, M., Colilla, M., Ruiz-Hitzky, E., 2003. Biopolymer–clay nanocomposites based on chitosan intercalated in montmorillonite. Chem. Mater. 15, 3774–3780.

Dollery, S.C., 1991. Therapeutic Drugs. Churchill Livingstone, Edinburgh, pp. P272–P278.

El-Kamel, A., Sokar, M., Naggar, V., Gamal, S.A., 2002. Chitosan and sodium alginate-based bioadhesive vaginal tablets. AAPS Pharm. Sci. 4 (4), 1–7.

Fan, Q., Shan, D., Xue, H., He, Y., Cosnier, S., 2007. Amperometric phenol biosensor based on laponite clay–chitosan nanocomposite matrix. Biosens. Bioelectron. 22, 816–821.

Felton, L.A., McGinity, J.W., 2002. Influence of insoluble excipients on film coating systems. Drug Dev. Ind. Pharm. 28, 225–243.

Flynn, G.L., Yalkowsky, S.H., Roseman, T.J., 1974. Mass transport phenomena and models: theoretical concepts. J. Pharm. Sci. 63, 479–510.

Gates, W.P., Komadel, P., Madejová, J., Bujdák, J., Stucki, J.W., Kirkpatrick, R.J., 2000. Electronic and structural properties of reduced-charge montmorillonite. Appl. Clay Sci. 16, 257–271.

Günister, E., Pestreli, D., Ünlü, C.H., Atıcı, O., Güngör, N., 2007. Synthesis and characterization of Chitosan–MMT biocomposite systems. Carbohydr. Polym. 67, 358–365.

Harish Prashanth, K.V., Kittur, F.S., Tharanathan, R.N., 2002. Solid state structure of chitosan prepared under different N-deacetylating conditions. Carbohydr. Polym. 50, 27–33.

Hejazi, R., Amiji, M., 2002. Stomach-specific anti-H. pyroli therapy I: preparation and characterization of tetracycline-loaded chitosan microspheres. Int. J. Pharm. 235, 87–94.

Hejazi, R., Amiji, M., 2003. Chitosan-based gastrointestinal delivery systems. J. Contr. Release 89, 152–165.

Holme, H.K., Davidsen, L., Kristiansen, A., Smidsrød, O., 2008. Kinetics and mechanism of depolymerization of alginate and chitosan in aqueous solution. Carbohydr. Polym. 73, 656–664.

Illum, L., 1998. Chitosan and its use as a pharmaceutical excipient. Pharm. Res. 15, 1326–1331.

Kamiya, H., Mitsui, M., Takano, H., Miyazaki, S., 2000. Influence of particle diameter on surface silanol structure, hydration force, and aggregation behavior of alkoxide-derived silica particles. J. Am. Ceram. Soc. 83, 287–293.

Kasaai, M.R., 2008. A review of several reported procedures to determine the degree of N-acetylation for chitin and chitosan using infrared spectroscopy. Carbohydr. Polym. 71, 497–508.

Khunawattanakul, W., Puttipipatkhachorn, S., Rades, T., Pongjanyakul, T., 2008. Chitosan–magnesium aluminum silicate composite dispersions: characterization of rheology, flocculate size and zeta potential. Int. J. Pharm. 351, 227–235.

Kibbe, H.A., 2000. Handbook of Pharmaceutical Excipients, 3rd ed. American Pharmaceutical Association, Washington.

Liu, K.H., Liu, T.Y., Chen, S.Y., Liu, D.M., 2007. Effect of clay content on electrostimulus deformation and volume recovery behavior of a clay–chitosan hybrid composite. Acta Biomater. 3, 919–926.

Nakano, N.I., Shimamori, Y., Umehashi, M., Nakano, M., 1984. Preparation and drug adsorption characteristics of activated carbon beads suitable for oral administration. Chem. Pharm. Bull. 32, 699–707.

Nunthanid, J., Puttipipatkhachorn, S., Yamamoto, K., Peck, G.E., 2001. Physical properties and molecular behavior of chitosan films. Drug Dev. Ind. Pharm. 27, 143–157.

Okhamafe, A.O., York, P., 1984. Effect of solids–polymer interaction on the properties of some aqueous-based tablet film coating formulation. II. Mechanical characteristics. Int. J. Pharm. 22, 273–281.

Patel, H.A., Somani, R.S., Bajaj, H.C., Jasra, R.V., 2007. Preparation and characterization of phosphonium montmorillonite with enhanced thermal stability. Appl. Clay Sci. 35, 194–200.

Pongjanyakul, T., 2009. Alginate-magnesium aluminum silicate films: importance of alginate block structures. Int. J. Pharm. 365, 100–108.

Pongjanyakul, T., Khunawattanakul, W., Puttipipatkhachorn, S., 2009. Physicochemical characterizations and release studies of nicotine–magnesium aluminum silicate complexes. Appl. Clay Sci. 44, 242–250.

Pongjanyakul, T., Priprem, A., Puttipipatkhachorn, S., 2005. Investigation of novel alginate–magnesium aluminum silicate microcomposite films for modified-release tablets. J. Contr. Release 107, 343–356.

Pongjanyakul, T., Puttipipatkhachorn, S., 2007. Sodium alginate–magnesium aluminum silicate composite gels: characterization of flow behavior, microviscosity and drug diffusivity. AAPS Pharm. Sci. Technol. 8 (Article 72).

Puttipipatkhachorn, S., Nunthanid, J., Yamamoto, K., Peck, G.E., 2001. Drug physical state and drug-polymer interaction ob drug release from chitosan matrix films. J. Contr. Release 75, 143–153.

Ray, S.S., Okamoto, M., 2003. Polymer/layer silicate nanocomposites: a review from preparation to processing. Prog. Polym. Sci. 28, 1539–1641.

Remuñán-López, C., Bodmeier, R., 1997. Mechanical, water uptake and permeability properties of cross-linked chitosan glutamate and alginate films. J. Contr. Release 44, 215–225.

Remuñán-López, C., Portero, A., Vila-Jato, J.L., Alonso, M.J., 1998. Design and evaluation of chitosan/ethylcellulose mucoadhesive bilayered devices for buccal drug delivery. J. Contr. Release 55, 143–152.

Rhim, J.W., Hong, S.I., Park, H.M., Ng, P.K., 2006. Preparation and characterization of chitosan-based nanocomposite films with antimicrobial activity. J. Agric. Food Chem. 54, 5814–5822.

Rinaudo, M., 2006. Chitin and chitosan: properties and applications. Prog. Polym. Sci. 31, 603–632.

Ritthidej, G.C., Phaechamud, T., Koizumi, T., 2002. Moist heat treatment on physicochemical change of chitosan salt films. Int. J. Pharm. 232, 11–22.

Rojtanatanya, S., Pongjanyakul, T., 2010. Propranolol–magnesium aluminum silicate complex dispersions and particles: characterization and factors influencing drug release. Int. J. Pharm. 383, 106–115.

Ruiz-Hitzky, E., Darder, M., Aranda, P., 2005. Functional biopolymer nanocomposites based on layered solids. J. Mater. Chem. 15, 3650–3662.

Sánchez-Martin, M.J., Sánchez-Camazano, M., Vicente-Hernández, M.T., Dominguez-Gil, A., 1981. Interaction of propranolol hydrochloride with montmorillonite. J. Pharm. Pharmacol. 33, 408–410.

Senel, S., İkinci, G., Kaş, S., Yousefi-Rad, A., Sargon, M.F., Hincal, A.A., 2000. Chitosan films and hydrogels of chlorhexidine gluconate for oral mucosal delivery. Int. J. Pharm. 193, 197–203.

Sinko, P.J., 2006. Matin's Physical Pharmacy and Pharmaceutical Sciences, 5th ed. Lippincott Williams & Wilkins, Philadelphia.

Sriamornsak, P., Kennedy, R.A., 2008. Swelling and diffusion studies of calcium polysaccharide gels intended for film coating. Int. J. Pharm. 358, 205–213.

Terzyk, A.P., Rychlicki, G., Biniak, S., Łukaszewicz, J.P., 2003. New correlations between the composition of the surface layer of carbon and its physicochemical properties exposed while paracetamol is adsorbed at different temperature and pH. J. Colloid Interf. Sci. 257, 13–30.

Thacharodi, D., Panduranga Rao, K., 1993. Release of nifedipine through crosslinked chitosan membranes. Int. J. Pharm. 96, 33–39.

Tuovinen, L., Peltonen, S., Järvinen, K., 2003. Drug release from starch-acetate films. J. Contr. Release 91, 345–354.

Wang, S.F., Shen, L., Tong, Y.J., Chen, L., Phang, I.Y., Lim, P.Q., Liu, T.X., 2005. Biopolymer chitosan/montmorillonite nanocomposites: preparation and characterization. Polym. Degrad. Stabil. 90, 123–131.

Wang, X., Du, Y., Luo, J., Lin, B., Kennedy, J.F., 2007. Chitosan/organic rectorite nanocomposite films: structure, characteristic and drug delivery behaviour. Carbohydr. Polym. 69, 41–49.

Wang, X., Du, Y., Yang, J., Wang, X., Shi, X., Hu, Y., 2006. Preparation, characterization and antimicrobial activity of chitosan/layered silicate nanocomposites. Polymer 47, 6738–6744.

Zhao, X., Mai, Z., Kang, X., Zou, X., 2008. Direct electrochemistry and electrocatalysis of horseradish peroxidase based on clay–chitosan–gold nanoparticle nanocomposite. Biosens. Bioelectron. 23, 1032–1038.